Supplementary Methods and Results for:

Impact of non-brain anatomy and coil orientation on inter- and intra-subject variability in TMS at midline

Erik G. Lee[1,2], P. Rastogi[2], R. L. Hadimani[3,2], and D. C. Jiles[2], Joan A. Camprodon[1]

1. *Laboratory for Neuropsychiatry and Neuromodulation, Department of Psychiatry, Massachusetts General Hospital, Harvard Medical School, Charlestown, Massachusetts 02129*
2. *Department of Electrical and Computer Engineering, Iowa State University, Ames, Iowa, 50011, USA*
3. *Department of Mechanical and Nuclear Engineering, Virginia Commonwealth University, Richmond, Virginia, 23284, USA*

Corresponding author's email: erik.lee.mn@gmail.com

Model Development

The models used in this study were developed using structural T1 and T2 weighted MRI images from the structural preprocessed package of the Human Connectome Project's (HCP) 900 Subject release (Van Essen et al., 2012). These images have isotropic resolution of 0.7 mm, which has been shown to allow for more accurate surface reconstruction than with more standard 1.0 mm isotropic voxels (Lin and Scott, 2012). Further all HCP images used for model development were graded to have "good" or "excellent" quality as determined by HCP staff (as all images in the 900 subject release) with grading metrics outlined in (Marcus et al., 2013). Further modifications to the original MRI images were made by the HCP team as a part of the release, to blur the facial region and area around the ears which aids in the de-identification of derived head models.

In total, SimNIBS generates finite element compatible surfaces for skin, skull, CSF, grey matter, white matter, ventricles and cerebellum (Thielscher et al. 2015). SimNIBS utilizes FreeSurfer to generate surfaces for grey matter, white matter, and cerebellum (Fischl et al. 1999), and FSL to segment surfaces for skin, skull, cerebrospinal fluid (CSF), and ventricles (Smith, 2002). See **Suppl. Fig. 1** for example anatomy from a single model. The inferior bounds of the models used in this study occurred below the most inferior region of the brain, approximately at mouth level, which is sufficiently far from most common TMS targets to not effect simulation outcomes. More details from the creators of SimNIBS on generating the meshed triangles for the models can be found in a recent publication from Windhoff et. al (Windhoff et al. 2013).

Each anatomical surface that makes up a model represents the outer boundary of the anatomy specified. Because of this, the inner boundaries of tissues (except for ventricles and cerebellum who have no inner boundaries) are defined by the outer boundaries of the next, smaller tissue. For example, the inner boundary of the skin is defined by the outer boundary of the skull, the inner boundary of skull is defined by the inner boundary of CSF, the inner boundary of CSF is defined by the outer boundary of grey matter, etc. For TMS, since stimulation occurs mainly over superficial, cortical structures, this is a reasonable simplification which has also been used in other TMS studies (Opitz et al. 2016; Thielscher, et al. 2011; Krieg et al. 2015).

The SimNIBS pipeline is completely automated. Although automated reconstruction algorithms for the surfaces previously mentioned are relatively accurate, some models may have errors in specific surfaces. All models were inspected for surfaces that represent obvious, unrealistic anatomical geometries. The most common problem observed in head models was in the skull, where some models appeared to have very isolated divots that decreased the skull's thickness, replacing it with more skin. The other main problem appeared in the segmentation of the cerebellum, where small areas of the cerebellum protruded past the cerebellum's natural boundary and into the area defined as skull. Models with this problem in the segmentation of the cerebellum were excluded from the study. Simulations were conducted to test the effect of skull divots on the integrity of simulation results. Results (seen in the Skull Defects section of the Supplementary Methods and Results) highlight one of the most severe cases of these skull divots and illustrate that the E-Field profile is not adversely effected by this artifact, and thus models with this artifact were included in the study.

Supplementary Figure 1: View of different anatomical components of example model.

Additional Simulation Details

The Magstim 70 mm Figure-8 coil was approximated as a series of infinitely thin, current carrying loops. The coil was designed with each winding having 9 turns with an inner radius of 56 mm, and an outer radius of 87 mm with equal spacing between turns (Hovey and Jalinous, 2006). The coil windings were placed 5 mm above the surface of the skin to account for coil casing. The anatomical coil placement of the vertex was identified by shifting the models so that the center of the coil is an equal distance from the left and right outer bounds of the skull. Further, the anterior and posterior location of the scalp was localized by finding the most superior part of the anterior commissure – posterior commissure aligned head models. Simulations were ran utilizing a quasi-static, low frequency solver for calculating the electromagnetic fields generated from the coil, using the same procedure as previous work from our group (Crowther et al. 2014).

The original models developed using SimNIBS, were in ASCII stereolithography (STL) format. Using the same anatomical hierarchy structure described in the model development section of the supplementary methods and results, SEMCAD X (SEMCAD X, 2014) used the STL files generated from

SimNIBS to sample voxels into a uniform rectilinear grid. Simulations were carried out with 1 mm^3 isotropic, cubic voxels. Each voxel was assigned to a specific segmented anatomy and then assigned an electrical conductivity and relative permittivity based on a standard set of previously published values (Hasgall et al., 2012) and seen in **Suppl. Table 1**. The main reason for running these simulations in SEMCAD X instead of SimNIBS is the flexibility of post-processing within SEMCAD X, and the ability to have simulation results in a rectilinear grid.

Tissue	*Permittivity*	*Electrical Conductivity (S/m)*
Cerebellum	7.84×10^{4}	1.24×10^{-1}
Cerebrospinal Fluid	1.09×10^{2}	2.00
Grey Matter	7.81×10^{4}	1.04×10^{-1}
Skin	1.14×10^{3}	2.00×10^{-4}
Skull	1.44×10^{3}	2.03×10^{-2}
Ventricles	1.09×10^{2}	2.00
White Matter	3.43×10^{4}	6.45×10^{-2}

Supplementary Table 1: The permittivity and electrical conductivity used for each model component.

Skull Defects

To test the effects of skull divots on E-Field calculations, a single model with an extreme case of a skull divot was edited using the free mesh editing software MeshMixer (Schmidt and Singh, 2010) to make the outline of the skull follow what the expected contours of the human skull should be. The original skull and edited skull can be seen in **Suppl. Fig. 2** on the left and right, respectively. In the unedited skull, the divot will be made up of voxels with the electrical properties of skin, and in the edited case, the skull will have the normal electrical properties (of skull). Identical simulations were then run on both models and results were exported to Matlab for post-processing.

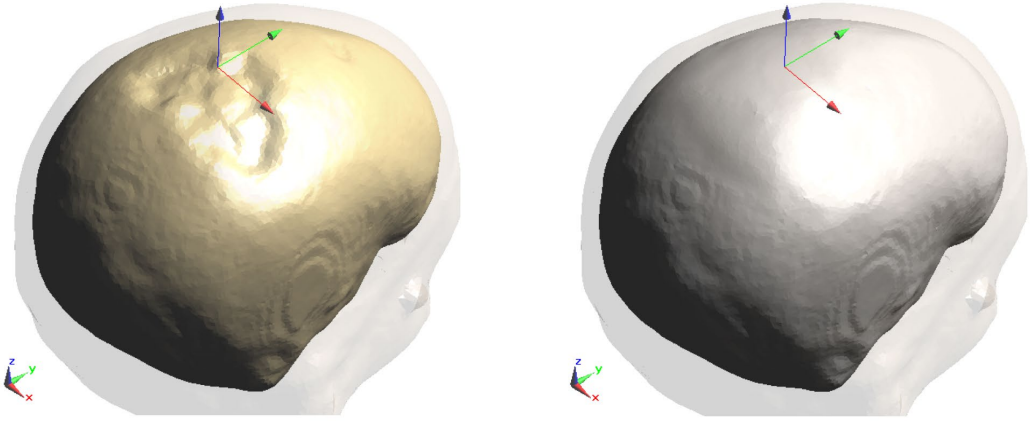

Supplementary Figure 2: Original model with divot on left, fixed model edited by MeshMixer on right.

Seen in **Suppl. Fig. 3** is the surface view of the induced E-Field in grey matter for the original, unedited model (left), and the edited model (right). Visual inspection of the results reveals no obvious differences between the two models. To further inspect the possible differences in the E-Field strength/distribution between the two models, results between the two simulations were compared on a per-voxel basis in Matlab, while only considering voxels in the brain. Results showed that the mean difference between the E-Field in the two models was 0.07 V/m per voxel. In comparison, the maximum stimulation intensity of over 200 V/m. The point in the brain with the greatest difference was only 1.22 V/m, which again is less than 1% of the maximum stimulation intensity. Further the V-Half (1 mm^3) metric was compared for both models and the error was less than 0.3%.

Since results show such a small difference between the original model and the edited model (less than 1% error), it was decided that models with this defect could be included in simulations without further editing. Future work could explore whether or not there is any value in segmenting the skin and skull separately.

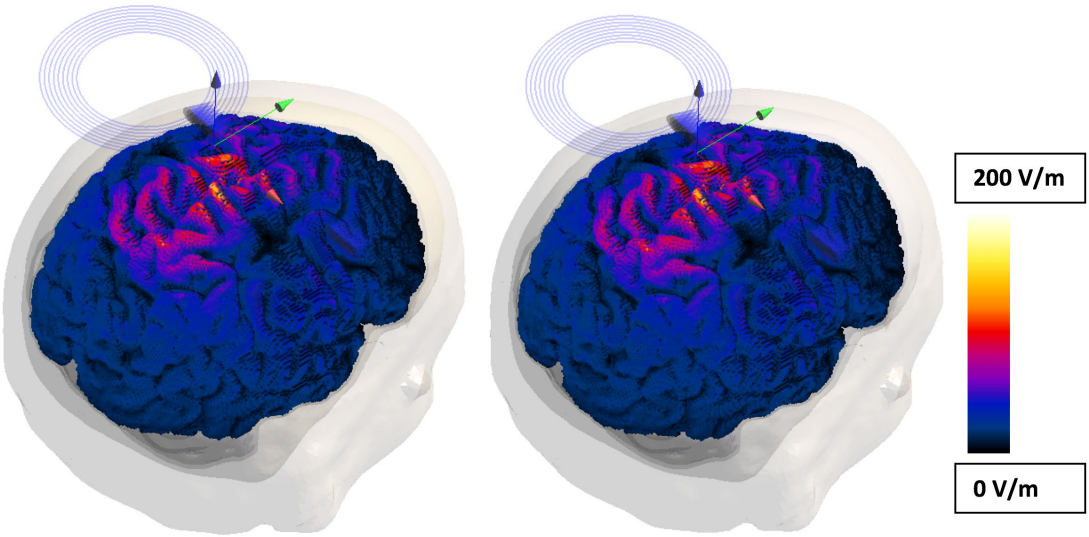

Supplementary Figure 3: Surface view of the electric field on the original model on left, and edited model on right.

Voxel Resolution and Staircasing Error

Previous literature has shown that calculations using rectilinear grids of voxels can be susceptible to numerical errors, specifically at the interfaces of tissues with different conductivities (Thielscher et al. 2011; Laakso and Hirata 2012). Because the interaction of CSF thickness with both stimulation intensity and the distribution of stimulation throughout the brain is of particular interest in this study, careful consideration must be made to ensure results are not merely an artifact of numerical errors.

In this study, the first step taken to reduce the likelihood of numerical inaccuracies was the incorporation of high-resolution voxels. The voxels used in this study were 1 mm isotropic, meaning that the mesh used in this study was 8 times as dense as those evaluated in previous works that have criticized rectilinear grids (i.e. 1 mm^3 vs. 8 mm^3) (Thielscher et al. 2011; Laakso and Hirata 2012). The second step, was to calculate measures at multiple scales of resolutions (i.e. E-Max, V-Half, location of maximum stimulation, see **Methods** section of main text). Throughout the results, we put the greatest emphasis on the 1 cm^3 E-Max and V-Half thresholds, because these rely on a greater number of voxels, making their

values less dependent on any given voxel that may be effected by numerical artifacts. After concluding the study, we also ran additional simulations at a voxel resolution of 0.5 mm isotropic to test the reproducibility of our final results. The voxels used in these final simulations would be 64 times as dense those used in previously cited works, and 8 times denser than the simulations used in the main results of our study. Simulations were reproduced in four models, two models with very thick CSF and two models with very thin layers of CSF at the site of stimulation.

A figure summarizing the results of these simulations can be seen below in **Suppl. Fig. 4**. These supplementary simulations show that for three out of the four models, computed E-Fields are very similar for all observed points in the brain. However, in one of the models (model 144832 with thin CSF), we see that the electric field has very large deviation in the 10 mm^3 of voxels in the brain with the greatest E-Field intensity. In this model, the deviation between the two sets of simulations is notably reduced from 10 mm^3 to 100 mm^3, and the E-Field intensities are approximately equivalent beyond 100 mm^3.

To specifically test how these differences in E-Field maps generated from two different voxel resolutions would affect E-Max and V-Half metrics, E-Max and V-Half metrics were calculated for the four new simulations. The results are displayed in **Suppl. Fig. 4**, showing that the E-Max 1 cm^3, and V-Half 1 cm^3 are very reliable (changes < 5%), especially when the extent of between-model variability seen in E-Max 1 cm^3 and V-Half 1 cm^3 is considered. As mentioned in the previous paragraph, model 144832 has markedly different E-Field estimates for the top 10 mm^3 of stimulated voxels. Because of this both the E-Max and V-Half 1 mm^3 metrics are not very reliable for this model (E-Max 1 mm^3 = 318 V/m normal resolution, and 502 V/m high resolution). For the three other models, both the original simulations and high-resolution simulations gave comparable results with smaller errors.

These outcomes show that as higher resolution voxels are used, which mimic the true geometry of the model more accurately, the 1 mm^3 thresholds are more susceptible to error and the 1 cm^3 thresholds are robust to the artifacts that effect the 1 mm^3 thresholds. Further, for all the models tested, any small errors observed between the 1 mm simulations and the 0.5 mm simulations are much smaller than the differences observed between the models with thick CSF and the models with thin CSF.

Based on these results, we would suggest that future works using rectilinear voxels and looking for thresholding schemes either use a metric comparable to E-Max 1 cm^3, or the field of the voxel whose E-Field intensity is greater than all but the top ~100 mm^3's worth of voxels in the brain.

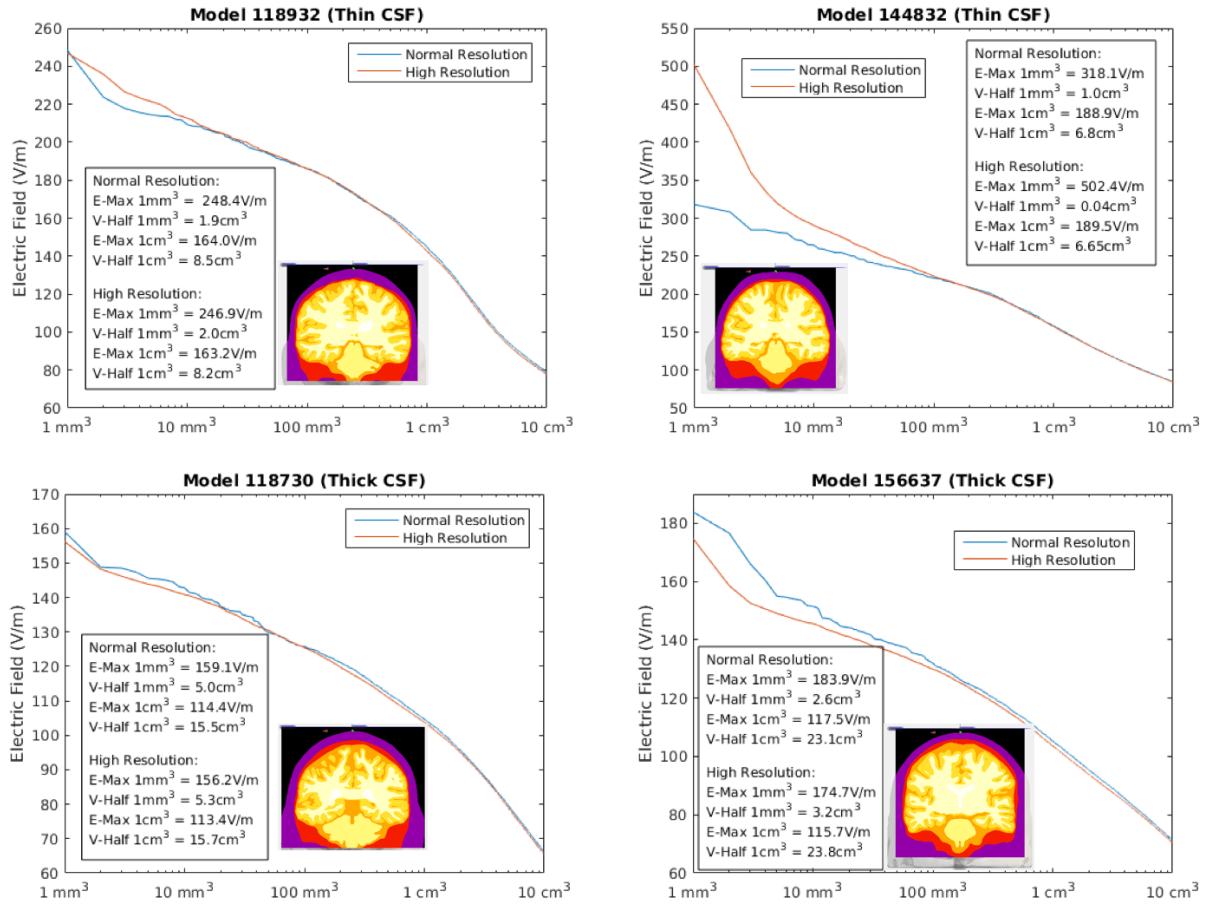

Supplementary Figure 4: Comparison of E-Field calculations of normal simulations (i.e. 1 mm voxels), and high-resolution simulations (0.5 mm voxels). The two lines in each graph represent the electric field from the top 1 mm^3 of voxels receiving the greatest stimulation intensity to the top 10 cm^3 of voxels, with one line for each simulation. Note that this is not a cumulative average of the E-Field, but direct measurements of the E-Field that different degrees of peak voxels will experience. E-Max and V-Half metrics are also presented at both normal- and high-resolution for each set of simulations.

Anatomical Variability in Models

As mentioned in the results and discussion section, differences in brain-scalp distance (BSD) and CSF thickness in our 50 model population are large enough to have significant effects on the induced E-Field. The distribution of BSD and CSF thickness can be seen in **Suppl. Fig. 5**. Results show that BSD is 2.0 centimeters on average and spans a range of over 1.5 (1.5-3.0) centimeters over the vertex. CSF similarly varies over 0.4 (0.3-0.7) centimeters and has a mean thickness of 0.5 centimeters over the vertex.

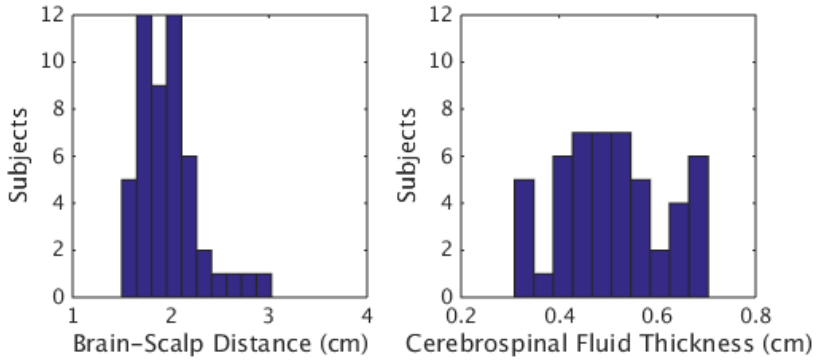

Supplementary Figure 5: Histograms outlining the distribution of BSD (left) and CSF Thickness (right) in the 50 models.

As seen in **Suppl. Fig. 6**, there is also significant variation in grey matter (GM) volume, white matter (WM) volume, CSF volume, and skull volume. Grey matter and white matter volume do not have any statistically significant relationship with E-Max or V-Half at any thresholds. There is a relationship with CSF and skull volume that is significantly related to E-Max and V-Half, due to their relationship with BSD and CSF thickness (see **Suppl. Fig. 7**).

Suppl. Fig. 7 outlines the relationships between different anatomical variables. The image shows that neither GM or WM volume are related to CSF thickness and BSD, such that variability of E-Max and V-Half are in no way normalized by the absolute volume of the brain. As previously mentioned, there is a strong correlation between BSD and overall skull volume, and also CSF thickness with CSF volume, such that some weak ability to predict E-Max and V-Half is given to skull volume and CSF volume.

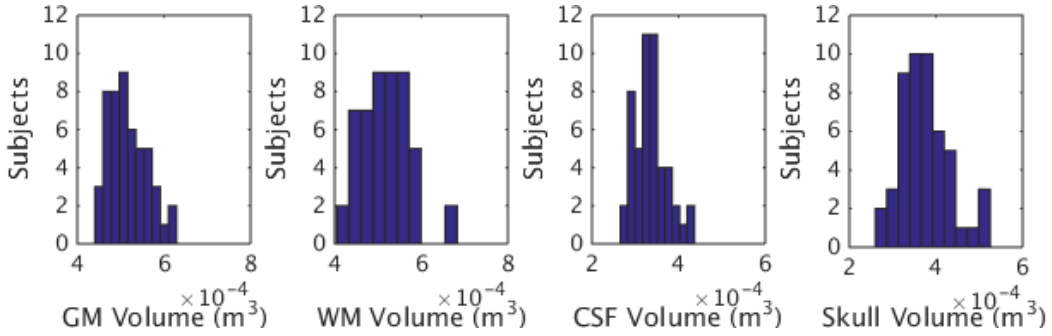

Supplementary Figure 6: Histograms outlining the distribution of Grey Matter Volume (far left), White Matter Volume (center left), Cortical CSF Volume (center right), and Skull Volume (far right) in the 50 models. Note that the x-axis scale is not the same in all plots.

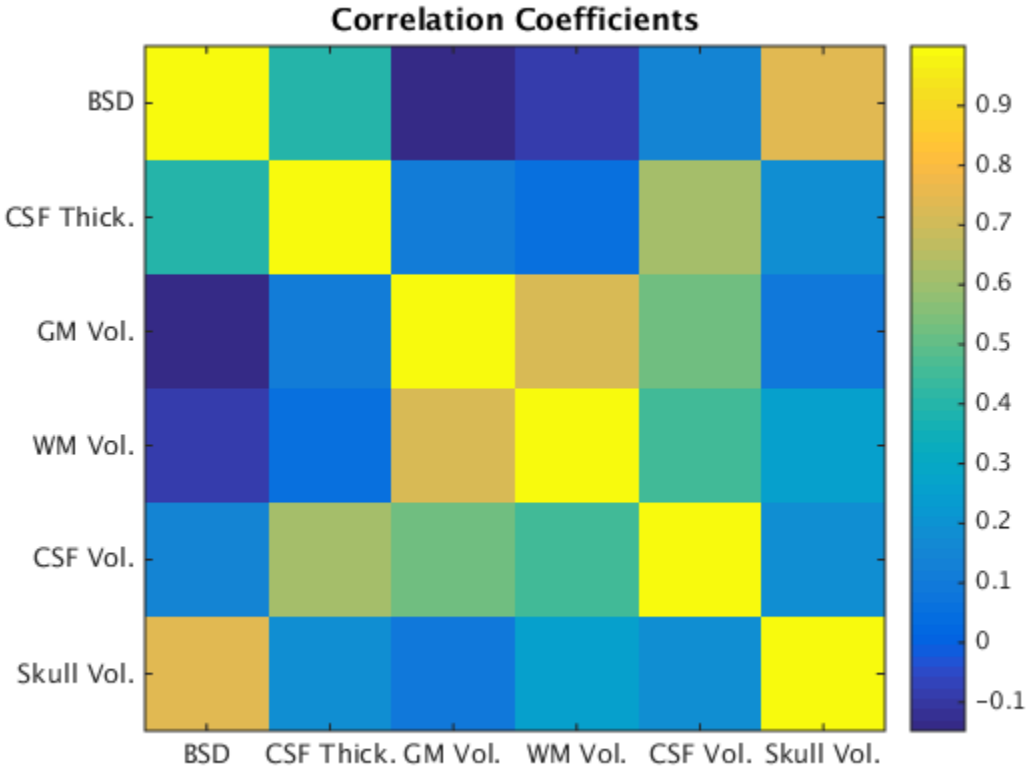

Supplementary Figure 7: Image plot displaying the correlation coefficients between different anatomical features. Color bar on right indicates the intensity of correlation coefficient for different shades.

E-Max and V-Half Variability

Suppl. Fig. 8 outlines the variability associated with different E-Max and V-Half thresholds. As expected, there is more variability seen within less conservative E-Max thresholds, such that a larger range of electric field values are observed. The same trend holds true for V-Half, but only after taking into account the relative magnitude of V-Half values at different thresholds.

It should be noted that although taking E-Max thresholds with a larger volume such as E-Max (1 cm^3) is more stable than that of E-Max (1 mm^3), and was shown to be valuable for statistical purposes in the main results of the paper, the E-Max (1 mm^3) threshold does not appear to have any outliers as may have been expected due to the voxel staircasing error (Laakso and Hirata, 2012). If similar simulations were ran with members of the Virtual Family (Christ et al., 2010), as have been previously used with our lab, it would be expected that there would be much more variability in E-Max (1 mm^3). It is possible that this is due to the additional supplementary tissues included in Virtual Family models, or it could also be due to CSF discontinuities in the Virtual Family models which are not present (at least in the STL files) for SimNIBS models.

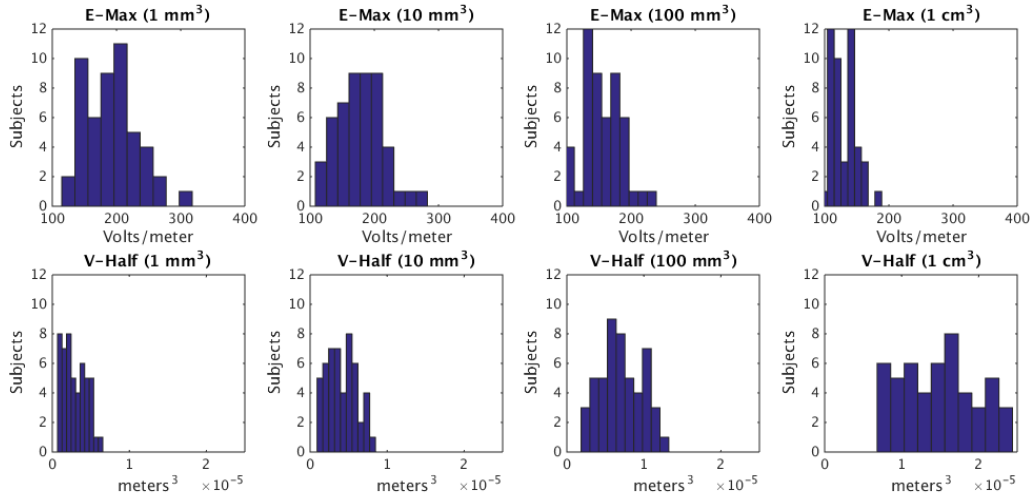

Supplementary Figure 8: Histograms showing the distributions for different E-Max and V-Half thresholds.

E-Max and V-Half with BSD and CSF:

In this section, we provide **Suppl. Figs. 9-11**, which are equivalent to **Fig. 4** in the main text, only now presented using the four different thresholding techniques, E-Max (1 mm^3), E-Max (10 mm^3), E-Max (100 mm^3), and E-Max (1 cm^3). It can be seen that all thresholds provide similar information when correlated with BSD and CSF. The less stable thresholding techniques (i.e. E-Max and V-Half 1 mm^3) have the weakest relationships with BSD and CSF, and the more stable thresholding techniques have the greatest relationships.

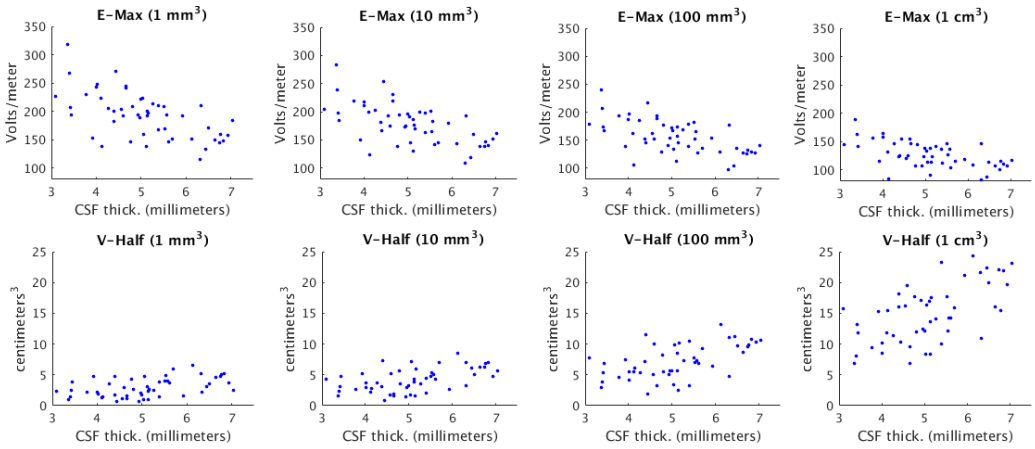

Supplementary Figure 9: In the top row, scatter plots include E-Max (V/m) at different thresholds plotted against BSD. In the bottom row, scatter plots include V-Half (cm^3) at different thresholds plotted against BSD. Results highlight how greater BSD is correlated with both weaker stimulation intensities and greater stimulation volume.

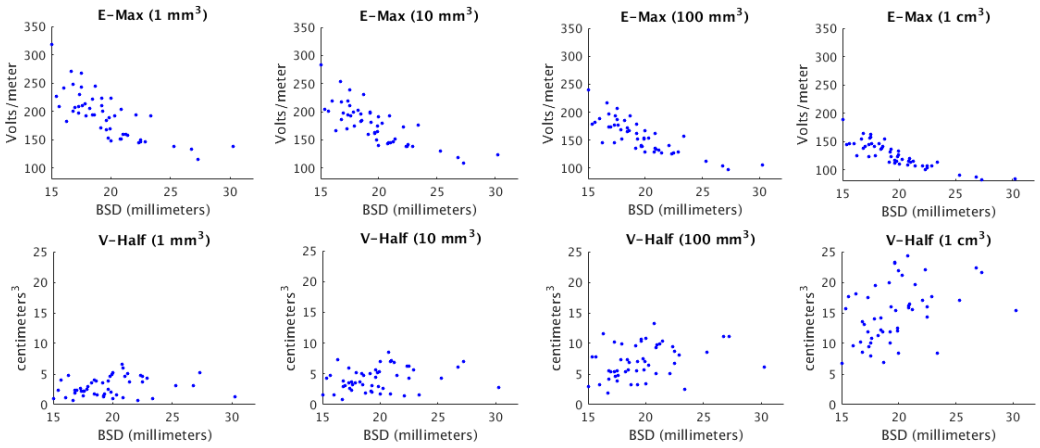

Supplementary Figure 10: In the top row, scatter plots include E-Max (V/m) at different thresholds plotted against CSF thickness. In the bottom row, scatter plots include V-Half (cm^3) at different thresholds plotted against CSF thickness. Results highlight how greater CSF thickness is correlated with both weaker stimulation intensities and greater stimulation volume.

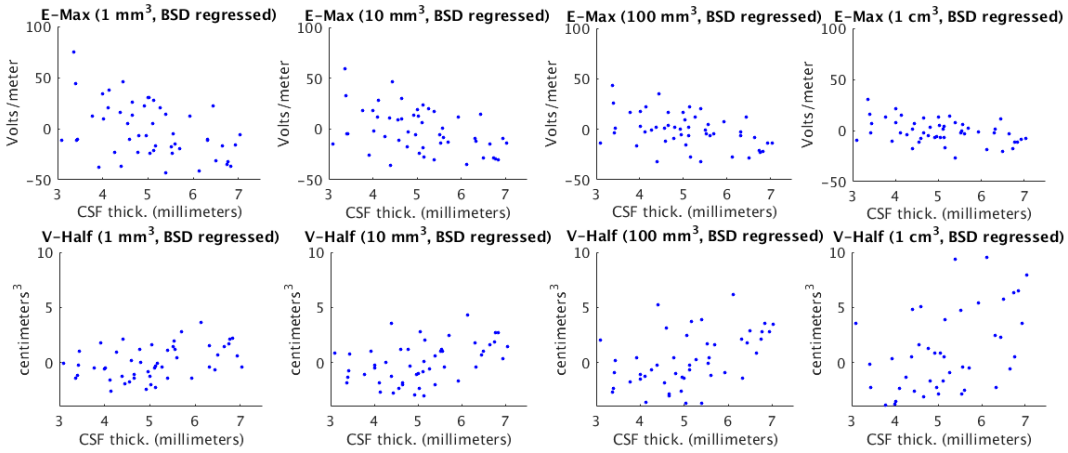

Supplementary Figure 11: In the top row, scatter plots include the E-Max (V/m) at different thresholds that is not explained by BSD (which has been accounted for through linear regression), plotted against CSF thickness. In the bottom row, scatter plots include the V-Half (cm^3) at different thresholds that is not explained by BSD, plotted against CSF thickness. Results highlight how greater CSF thickness is correlated with both weaker stimulation intensities and greater stimulation volume, even after accounting for the effects of overall BSD.

Volume Stimulated with Absolute Thresholds

Shown below in **Suppl. Figs. 12-14**, are plots highlighting variability in simulation outcomes for absolute thresholds, rather than the relative (normalized) thresholds discussed in the main section of the paper. First seen in **Suppl. Fig. 12**, are histograms highlighting the distribution of volume stimulated over four different absolute electric field thresholds (50, 75, 100, and 125 V/m) for the 50 models. **Suppl. Fig. 13** and **Suppl. Fig. 14** highlight how these distributions are predicted by brain scalp distance and CSF thickness respectively. Brain scalp distance had the greatest predictive value for estimating the volume of the brain stimulated above 75 V/m ($r = -0.91$, $p < 0.001$) (in comparison to other thresholds). Further CSF thickness had the greatest predictive value for estimating the volume of the brain stimulated above 125 V/m ($r = -0.62$, $p < 0.001$). It should be noted, that absolute thresholds are not able to give insight into the relative spread of stimulation in cases where the maximum stimulation is scaled to be equivalent in all models, which would be representative of the V-Half and A-Half thresholds outlined in the main body of the paper. Because of this, the volume stimulated above these absolute thresholds will be very strongly tied to the overall stimulation intensity (E-Max). This is illustrated by the strong relationship between E-Max (1 cm^3) and both the volume of the brain stimulated over 100 and 125 V/m ($r > 0.9$ for both cases). Still though, for unique scenarios where TMS is applied in such a way that all individuals receive the same stimulation intensity (again as defined by percent maximum stimulator output), these results highlight the expected inter-subject variability and their relationship to both BSD and CSF thickness.

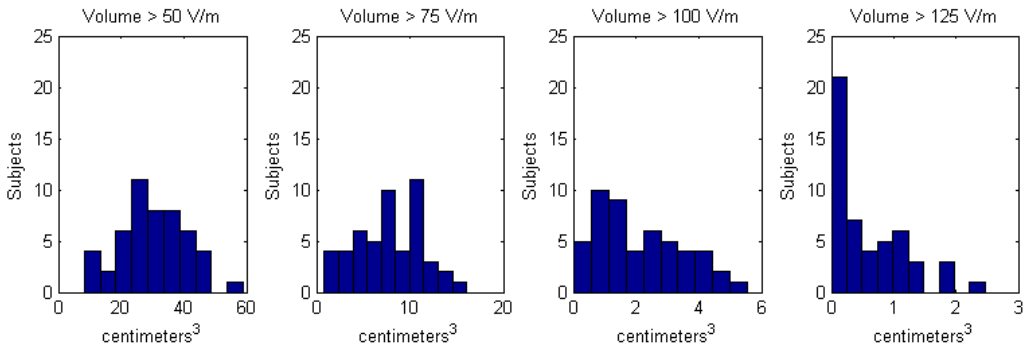

Supplementary Figure 12: Four histograms showing the total volume of the brain stimulated over 50 (far left), 75 (center left), 100 (center right), and 125 (far right) V/m in all the 50 models.

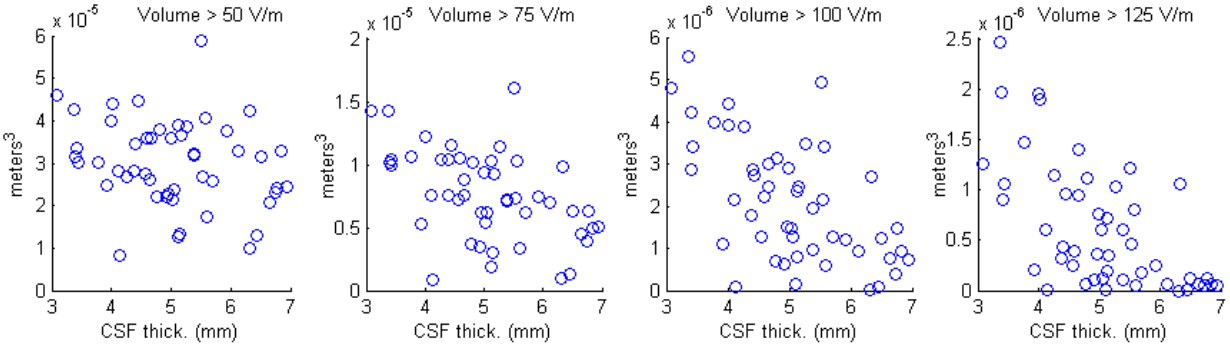

Supplementary Figure 13: Four scatter plots showing the relationship between BSD and the volume of the brain stimulated over 50 (far left), 75 (center left), 100 (center right), and 125 (far right) V/m. Note that the y-axis is not held constant between subplots for visualization purposes.

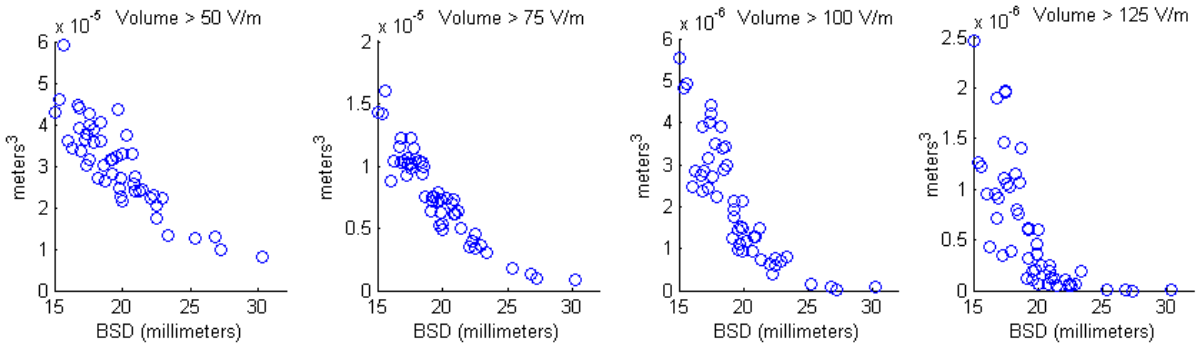

Supplementary Figure 14: Four scatter plots showing the relationship between CSF thickness and the volume of the brain stimulated over 50 (far left), 75 (center left), 100 (center right), and 125 (far right) V/m. Note that the y-axis is not held constant between subplots for visualization purposes.

Surface Stimulation:

The relationship between A-Half (1 cm^3) and both CSF thickness and BSD is similar to that of V-Half. Seen in **Suppl. Fig. 15**, A-Half (1 cm^3) is shown to increase as both BSD and CSF thickness increase ($p < 0.001$ for CSF and $p = 0.002$ for BSD). As with V-Half, CSF thickness remains a greater predictor of A-Half than BSD. This may be expected as A-Half (1 cm^3) and V-Half (1 cm^3) are very strongly correlated ($r = 0.98$, $p < 0.001$).

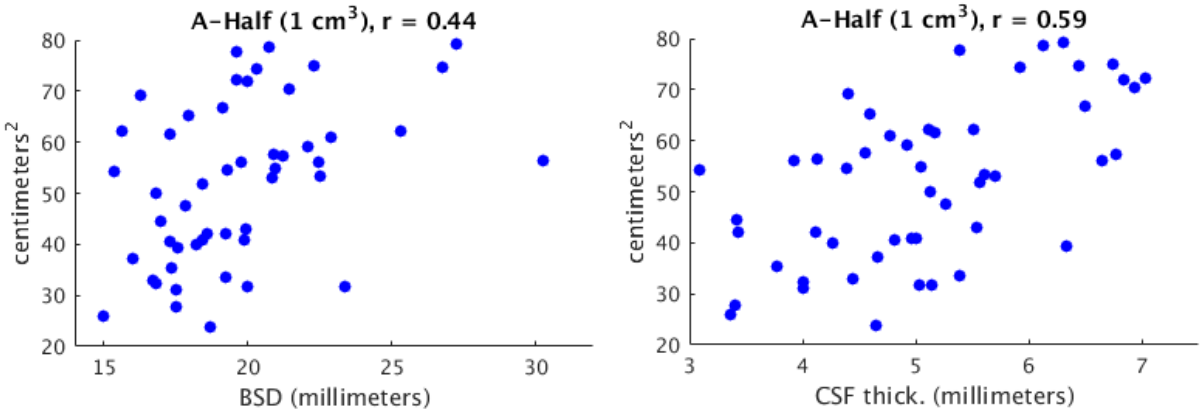

Supplementary Figure 15: Scatter plot comparing the relationship between the surface area (cm^2) of the brain receiving stimulation at intensities at least half of E-Max (1 cm^3) with BSD on left, and the surface area (cm^2) receiving the same stimulation with CSF thickness on right.

References

Christ A, Kainz W, Hahn EG, Honegger K, Zefferer M, Neufeld E, et al. The Virtual Family--development of surface-based anatomical models of two adults and two children for dosimetric simulations. Phys Med Biol 2010;55:N23–38. doi:10.1088/0031-9155/55/2/N01.

Crowther LJ, Hadimani RL, Jiles DC. Effect of Anatomical Brain Development on Induced Electric Fields During Transcranial Magnetic Stimulation. IEEE Trans Magn 2014;50.

Van Essen DC, Ugurbil K, Auerbach E, Barch D, Behrens TEJ, Bucholz R, et al. The Human Connectome Project: A data acquisition perspective. Neuroimage 2012;62:2222–31. doi:10.1016/j.neuroimage.2012.02.018.

Fischl B, Sereno MI, Dale AM. Cortical surface-based analysis I. Segmentation and Surface Reconstruction Anders. Neuroimage 1999;194:179–94. doi:10.1006/nimg.1998.0395.

Hasgall PA, Neufeld E, Gosselin MC, Klingenböck A, Kuster N. IT'IS database for thermal and electromagnetic parameters of biological tissues, version 2.2. July 11th 2012.

Hovey C, Jalinous R. THE GUIDE TO MAGNETIC STIMULATION. Whitland, Wales: Magstim; 2006.

Krieg TD, Salinas FS, Narayana S, Fox PT, Mogul DJ. Computational and experimental analysis of TMS-induced electric field vectors critical to neuronal activation. J Neural Eng 2015;12:46014. doi:10.1088/1741-2560/12/4/046014.

Laakso I, Hirata A. Reducing the staircasing error in computational dosimetry of low-frequency electromagnetic fields. Phys Med Biol 2012;57:25–34. doi:10.1088/0031-9155/57/4/N25.

Lin GG, Scott JG. The Minimal Preprocessing Pipelines for the Human Connectome Project. Neuroimage 2012;100:130–4. doi:10.1016/j.pestbp.2011.02.012.Investigations.

Marcus DS, Harms MP, Snyder AZ, Jenkinson M, Anthony J, Glasser MF, et al. Human Connectome Project Informatics: quality control, database services, and visualization. Neuroimage 2013;80:202–19. doi:10.1016/j.neuroimage.2013.05.077.Human.

Opitz A, Fox MD, Craddock RC, Colcombe S, Milham MP. An integrated framework for targeting functional networks via transcranial magnetic stimulation. Neuroimage 2016;127:86–96. doi:10.1016/j.neuroimage.2015.11.040.

Schmidt R, Singh K. Meshmixer: An Interface for Rapid Mesh Composition. ACM SIGGRAPH 2010

Talks, New York, NY, USA: ACM; 2010, p. 6:1--6:1. doi:10.1145/1837026.1837034.
SEMCAD X S. Partner Engineering AG (SPEAG), version 14.8 Aletsch 2014.
Smith SM. Fast robust automated brain extraction. Hum Brain Mapp 2002;17:143–55. doi:10.1002/hbm.10062.
Thielscher A, Antunes A, Saturnino GB. Field modeling for transcranial magnetic stimulation: A useful tool to understand the physiological effects of TMS? Conf Proc IEEE Eng Med Biol Soc 2015;2015:222–5. doi:10.1109/EMBC.2015.7318340.
Thielscher A, Opitz A, Windhoff M. Impact of the gyral geometry on the electric field induced by transcranial magnetic stimulation. Neuroimage 2011;54:234–43. doi:10.1016/j.neuroimage.2010.07.061.
Windhoff M, Opitz A, Thielscher A. Electric field calculations in brain stimulation based on finite elements: An optimized processing pipeline for the generation and usage of accurate individual head models. Hum Brain Mapp 2013;34:923–35. doi:10.1002/hbm.21479.